Atmospheric Absorption versus Deep Ultraviolet (Pre-)Resonance in Raman LIDAR Measurements

Hans D. Hallen*[a], Adam H. Willitsford[b], Ryan R. Neely III[a], C. Todd Chadwick[a], C. Russell Philbrick[a]

[a]North Carolina State University, Department of Physics, Raleigh, NC, USA 27695-8202;
[b]Johns Hopkins University Applied Physics Laboratory, Laurel, MD USA 20709

ABSTRACT

The Raman scattering of several liquids and solid materials has been investigated near the deep ultraviolet absorption features corresponding to the electron energy states of the chemical species present. It is found to provide significant enhancement, but is always accompanied by absorption due to that or other species along the path. We investigate this trade-off for water vapor, although the results for liquid water and ice will be quantitatively very similar. An optical parametric oscillator (OPO) was pumped by the third harmonic of a Nd:YAG laser, and the output frequency doubled to generate a tunable excitation beam in the 215-600 nm range. We use the tunable laser excitation beam to investigate pre-resonance and resonance Raman spectroscopy near an absorption band of ice. A significant enhancement in the Raman signal was observed. The A-term of the Raman scattering tensor, which describes the pre-resonant enhancement of the spectra, is also used to find the primary observed intensities as a function of incident beam energy, although a wide resonance structure near the final-state-effect related absorption in ice is also found. The results suggest that use of pre-resonant or resonant Raman LIDAR could increase the sensitivity to improve spatial and temporal resolution of atmospheric water vapor measurements. However, these shorter wavelengths also exhibit higher ozone absorption. These opposing effects are modeled using MODTRAN for several configurations relevant for studies of boundary layer water and in the vicinity of clouds. Such data could be used in studies of the measurement of energy flow at the water-air and cloud-air interface, and may help with understanding some of the major uncertainties in current global climate models.

Keywords: resonance Raman, absorption, water vapor, Raman lidar, MODTRAN

1. INTRODUCTION

Raman spectroscopy has become a commonly used tool for substance identification [1-3], stress measurements [4], and material characterization. Signal levels in Raman are quite small due to its low cross section. Resonance Raman is sometimes used to boost the signal level, and occurs when the excitation laser is tuned to an absorption feature of the material to be studied. It is useful in increasing signal levels for trace species concentrations in a non-absorbing matrix, or for nanoscale studies, which are limited in both volume and number of molecules available [5-11]. Many studies have used fix laser wavelengths to study pre-resonance Raman, in which the Raman signal is enhanced, but the excitation is not resonant because the wavelength is not precisely at the absorption energy [12-17]. Our earlier studies [5, 8-11, 18-21] have tuned the excitation laser in fine steps across the absorption features of interest, and show that Raman resonances followed isolated molecule (vapor phase) absorption features in a liquid phase sample when excited at a phonon-allowed transition, and attributed the effect to the short timescale imposed on the process by the phonon requirement. The key trade-off concerning real signal levels is between the resonance gain, the natural dipole absorption/emission dependence of frequency, $(\nu)^4$, and absorption. In this paper, we investigate this competition for the specific case of remote measurement of water vapor in a LIDAR configuration. We find an equation to describe the pre-resonance Raman gain as a function of wavelength, and use MODTRAN6 to calculate the absorption as a function of wavelength. Three scenarios are considered: a study of water vapor along a horizontal path over a body of water for a short range (500 m) at sea level; a study of low clouds from the ground on a 2 km vertical path; and the study of clouds from a ridge at 2 km along a horizontal path at 2 km altitude. We find that the resonance does provide some net gain to wavelengths as short as 250 nm, but that for the case of water vapor with its high energy (150 nm) resonance, the gains

Laser Radar Technology and Applications XXI, edited by Monte D. Turner, Gary W. Kamerman, Proc. of SPIE Vol. 9832, 983210 · © 2016 SPIE
CCC code: 0277-786X/16/$18 · doi: 10.1117/12.2224149

are modest and, for longer path lengths, might be more easily compensated by higher power lasers at longer wavelengths. We expect that the gains would be much more significant when the absorption lies above 200 nm.

One of the primary unknowns in climate models is the energy flow near clouds and near water surfaces. Fast, accurate measurements of water vapor, along with temperature, aerosols and wind, could provide a basis for constraining models for the energy exchange in these environments, and thereby improve climate model accuracy. Water vapor Raman has also been shown to be a useful tracer of atmospheric events [22] in and near the planetary boundary layer. Most such measurements were made with relatively long range bins (~75 m) and relatively long averaging (~5 minutes), although these could be relaxed at the expense of measurement range. We investigate here if resonance Raman could provide sufficient signal enhancement that measurements of low clouds or thin marine layers could be conducted. These would require range bins of a few meters and averaging times of several seconds.

The enhancement is usually described qualitatively as due to the longer timescale of the resonance Raman process compared to normal Raman since the resonant case involves a real intermediate state rather than a virtual state. For the case of the virtual state, the timescale of the process is limited by the Heisenberg uncertainty principle, and is essentially instantaneous compared to the atomic motion. In [11,23], we found that the resonance Raman process can be very short when the excitation is tuned to a symmetry forbidden transition, although the resonance gain is still large. We attribute this to the fact that a phonon must be available to allow absorption at that energy, and this requires a resonance within the molecule itself, which is short-lived. We observe it as the resonance gain for a liquid sample associated with the vapor-phase absorption wavelengths rather than those associated with liquid phase absorption. When the process is fast compared to the time a molecule requires to interact with its neighbors, the molecule will appear to have vapor phase energy transitions. Note that the molecule itself sets the time scale, not the laser pulse length or the time to exchange energy with its neighbors. Also note that the molecule is not in the vapor phase, and will not appear so when probed with a longer-time process, such as absorption. The dielectric constant, defined in frequency, assumes a longer-time process and cannot be used to describe this short-time interaction. To contrast this case, we present data of resonance Raman of ice. We find resonance gain occurring in a broad wavelength excitation band, 220-270 nm. Absorption at these wavelengths is observed in ice, but not water vapor, which absorbs strongly at shorter wavelengths. The reduction of the absorption energy in ice is due to a shielding of the absorption-induced dipole by movement of the dipoles of its neighbors. In other words, absorption at that energy relies upon interaction with the neighboring molecules. We observe resonance at this feature of ice since it is an allowed absorption energy in ice; thus, the typical resonance Raman process is long compared to the interaction time with its neighbors.

2. METHODS

Raman measurements of both liquids and solids are made in a 90-degree geometry with laser incident from underneath the sample, so that there is no presence of vapor in the beam path for the liquid measurements [9-10]. The tunable deep-UV laser is based upon frequency doubling of the output of an optical parametric oscillator (OPO) (Uoplaz) pumped by the third harmonic of a Nd-YAG laser (Spectra Physics). As shown in Fig. 1(a), the Nd-YAG laser output is tripled and a Pellin-Broca prism used to choose only the third harmonic beam to enter the OPO section. The OPO uses a counter-rotating quartz rod outside the cavity to correct lateral motion of the beam induced by the rotation of the BBO nonlinear crystal during wavelength adjustment. One of two BBO crystals, also counter-rotating, is used to double the OPO output frequency. A Pellin-Broca prism is used to choose the wavelength and aim the beam. The usable DUV range of wavelengths is ~215 – 300 nm, with visible wavelengths from the non-doubled outputs and near infrared from the idler output. Since we are interested in enhancement of the Raman signals due to the resonance effect, we normalize all spectra for laser power and the non-resonant ν_0^4 dipole emission enhancement.

3. WATER (ICE) RAMAN RESONANCE

The Raman signals shown in Fig. 1 have the three-peak structure expected for ice [24-26]. The Raman signal in the visible (439 nm) is small, and is only slightly larger at 277 nm. It increases rapidly near 263 nm, then more slowly again until it decreases near 250 nm, and then continues to rise again. The increase in the Raman signals is not monotonic, as is evident in the figure. To illustrate these points, the areas under the Raman spectra in Fig. 1 are integrated, and the sums are plotted in Fig. 2.

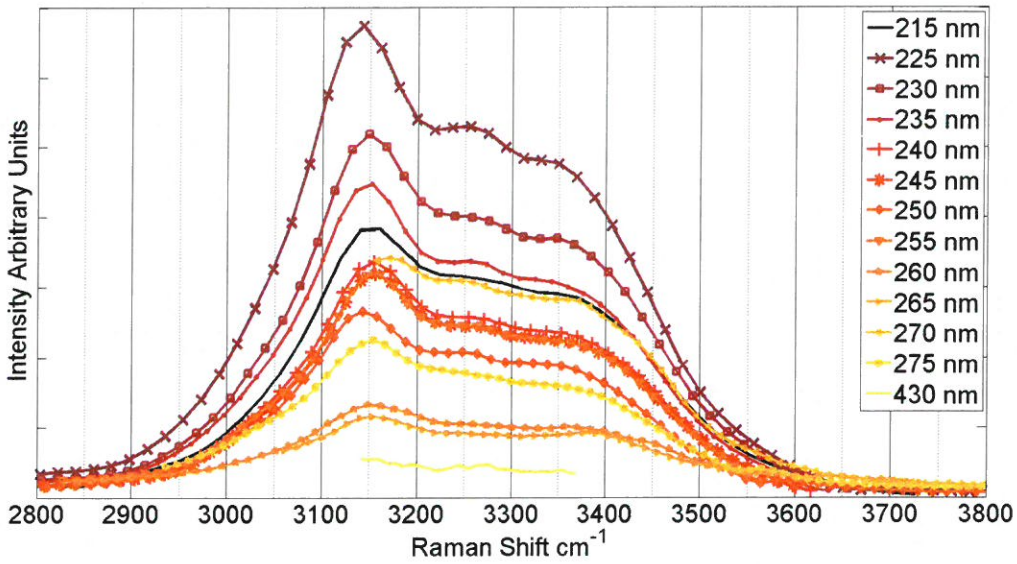

Figure 1. The UV Raman spectra of ice in small steps of excitation energy from 215 – 277.5 nm, and also the Raman spectra with excitation of 430 nm as a reference. Notice the steep increase to the peak value in the 10 nm step between 215 and 225 nm.

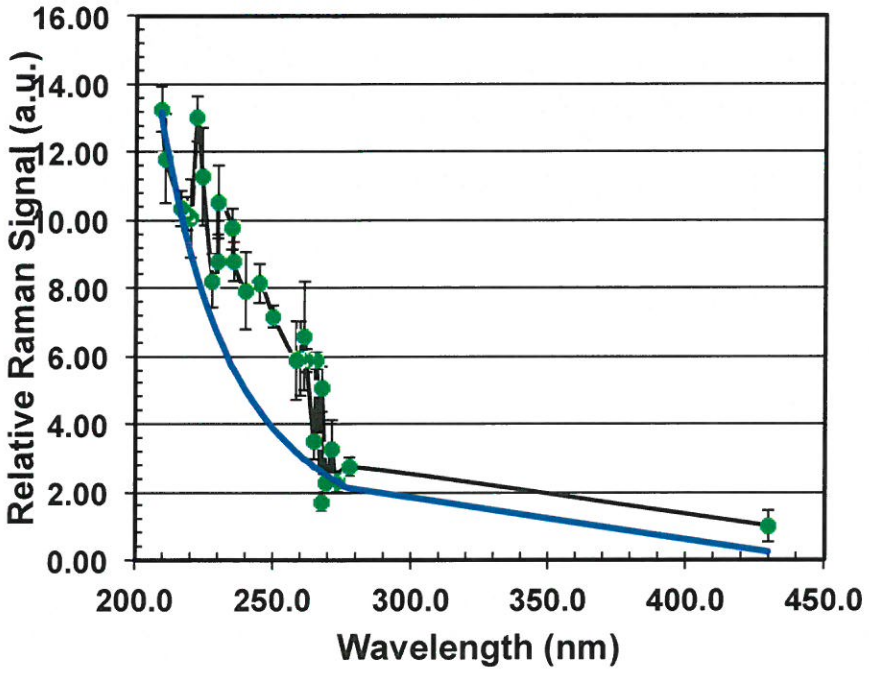

Figure 2. The area integrals of Raman spectra of ice from Fig. 1 for which the excitation energy is stepped in small increments from 215 – 277.5 nm, and also the integral of the Raman spectra with excitation of 430 nm as a reference.

The Raman wavelength dependence in Fig. 2 is increasing with decreasing wavelength. This is the pre-resonance for the strong absorption at ~150 nm in water. There is also a clear local structure in the 230-260 nm range. We investigate this

further by removing the background due to the pre-resonance. We fit the pre-resonance contribution and subtract it so that the resonance contribution can be observed directly. Usually, Raman scattering has intensity proportional to v_0^4 like dipole absorption/emission. A deviation from this proportionality occurs due to the 'A term' of the Raman scattering tensor α [10], so that as the frequency of the incident light approaches an electronic transition, the intensity I_{fi} for an initial, i, to final, f, state is given by

$$I_{fi} = \left(\frac{\pi}{\epsilon_0}\right)^2 (\nu_0 \pm \nu_{fi})^4 J_0 \sum_{\rho,\sigma} [\alpha_{\rho\sigma}]_{fi} [\alpha_{\rho\sigma}]^{\dagger}_{fi}, \quad (1)$$

where the sum is over all possible intermediate states, the resonant frequency is v_{fi}, and the input flux J_0. The alpha, polarizability tensor, components contain the resonance behavior. Usually, only one resonance will be important at a time, while the others provide a constant background. The sum then can be represented as two terms and

$$I \propto C[(2\nu_a)^2/(\nu_a^2 - \nu_0^2)^2] + D, \quad (2)$$

where C and D are proportionality constants that contain the v_0^4 dependence, and v_a is the representative excitation frequency between the ground state and electronic state. D is the term corresponding to the non-active states and is found to be relatively unimportant here. The solid line in Fig. 2 is a fit to equation (2), and is subtracted to arrive at Fig. 3. The representative excitation frequency, v_a, is 146 nm. This corresponds closely to the first major peak in the far UV absorption of water at 150 nm.

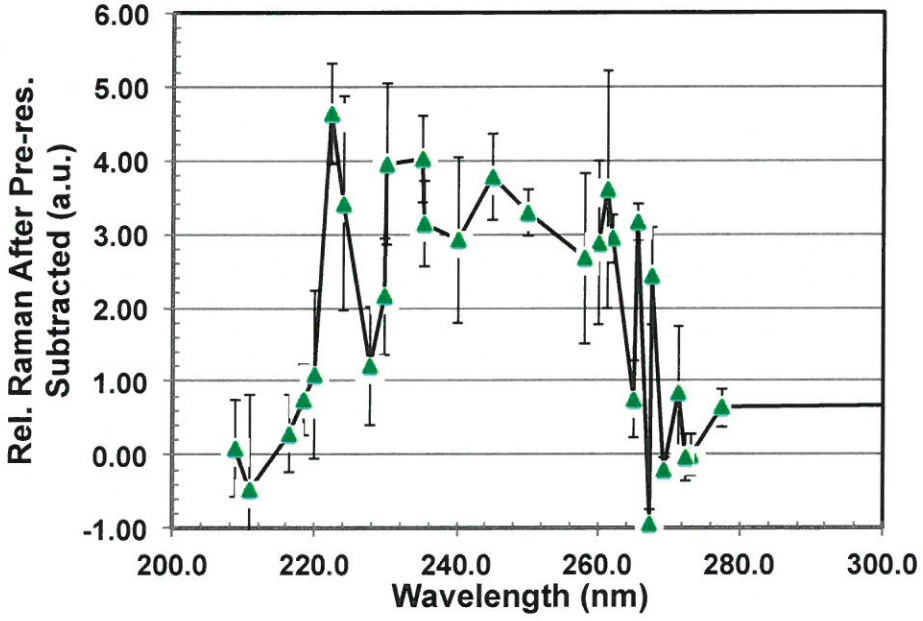

Figure 3. The resonance from the ice absorption in the wavelength region studied, obtained by subtracting the fitted resonance gain from the 146 nm ice absorption in Fig. 2.

This resonantly enhanced band ~222 nm and from 230-265 nm correlates well to the absorption curve of ice, but there is no corresponding absorption at these wavelengths for water vapor. Thus, the absorption band we observe is a solid-state effect. In fact, the energy lowering of the absorption is due to re-arrangement of the neighboring dipoles to reduce the energy of the excited state via a reduction of the field extent of the induced dipole. This resonant band will not be present in water vapor so we do not include it in the modeling. Instead, the fit pre-resonance curve will be used to estimate the resonance gain in water vapor for this spectral region.

4. WATER VAPOR RAMAN GAIN COMPARED TO THAT AT 532 NM

Now that the resonance properties for water have been determined, the fourth power of the frequency known, we turn to MODTRAN and the comparison of expected Raman intensity in the UV compared to that measured in the visible at 532 nm. We use the three cases described above, and default parameters for MODTRAN with the 1976 Standard U.S. Atmosphere, and rural aerosols with 23 km visibility. We obtain the results in Fig. 4.

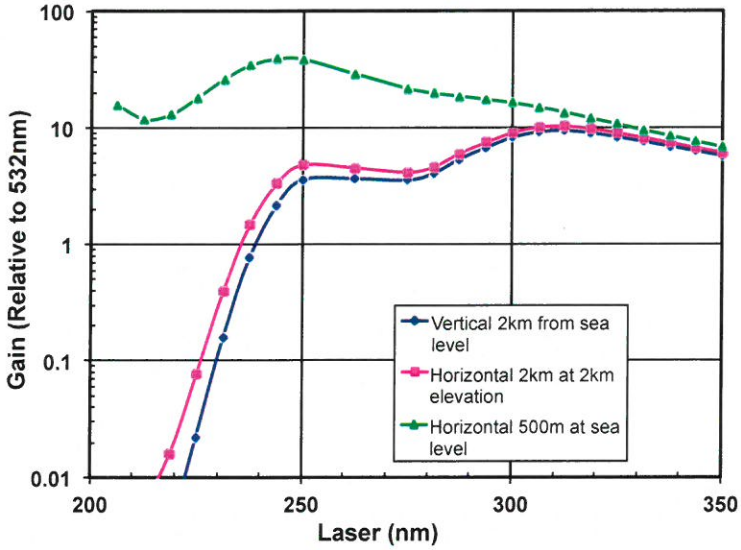

Figure 4. The expected Raman signal from water vapor in the UV compared to that at 532 nm by taking the ratio of the wavelength dependent UV Raman signal to that at 532 nm for three scenarios.

The short path scenario shows a generally increasing trend with shorter wavelength until ~250 nm, then begins decreasing as absorption becomes more important. The maximal gain of ~40 times is sufficient for the purposes of studying rapidly varying (tens of seconds) phenomena at the few meters length scale as noted above. The longer scenarios are much more disappointing, reaching a real signal gain of only about ten times near 310 nm. The double-humped functional form observed indicates that more than one species is important, see Fig 5.

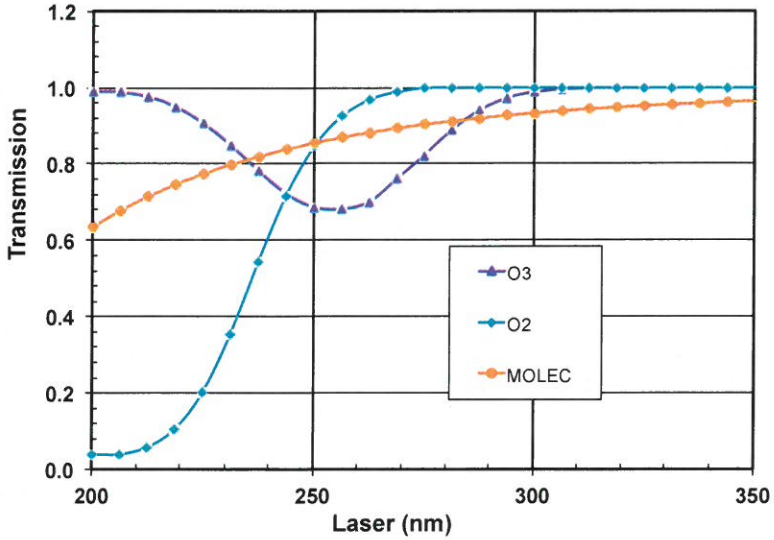

Figure 5. The MODTRAN-calculated path absorption for the 500 m long path at sea level for the species that determine the important extinctions in this study: ozone, oxygen, and molecular scatter.

Figure 5 shows the path extinctions for the relevant atmospheric constituents in this wavelength range. Shorter wavelengths are more sensitive to molecular scatter than longer wavelengths, and thus a general decrease of transmission with decreasing wavelength is found. The ozone Hartley absorption band is shown in the figure, centered a little above 250 nm. Oxygen displays the onset of the Herzberg continuum at slightly shorter wavelengths. It is the oxygen and ozone absorptions, combined with the generally increasing resonance and dipole trends that give the double-maxima observed in the longer range simulations.

We now examine the sensitivity of these results to changes that may occur in realistic scenarios. We begin with simulation results for increased water vapor content, from the ~46% relative humidity (RH) of the 1976 Standard Atmosphere (USSA76) to the saturated 100% RH at ground level. We expect no significant change in the gain since we are in the pre-resonance, not resonance, i.e. absorption band, regime for water absorption. The change in water vapor is made multiplicatively to the entire USSA76 water vapor profile, and the results are shown in Fig. 6.

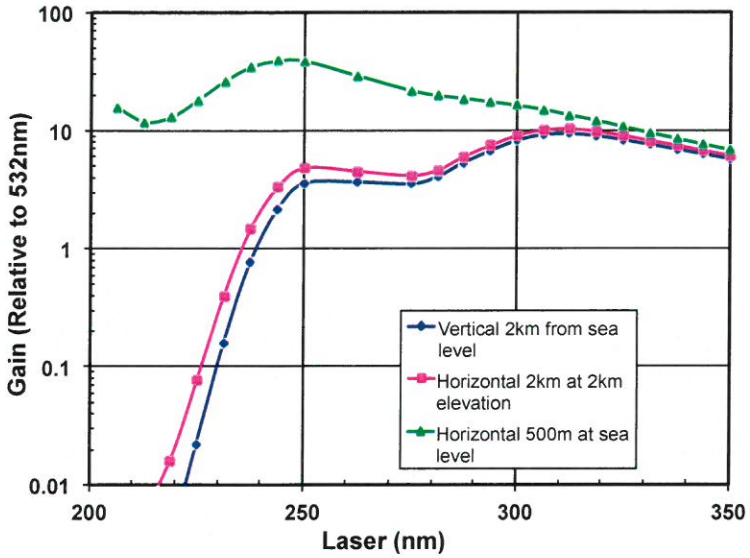

Figure 6. The effects of increased relative humidity (none) on resonance gain in the presence of atmospheric absorption.

As expected, no changes are observed upon increased RH, but the part of the spectrum over which ozone absorbs is strongly changed for increased ozone concentration, Fig. 5. This illustrates a problem with a simple measurement of water vapor by Raman at these wavelengths for excitation. If the Raman shifted light is absorbed at a different rate than the Raman line used for normalization of laser power due to extinction along the path, etc., as may be the case since water has a relatively high energy vibration energy, then ozone will effect the measurement, so it must also be measured and a correction made. The nature of the correction depends upon the particular laser wavelength chosen.

Next, we examine the influence of ozone on the relative signal gain. We wish to use a realistic ozone profile when the ozone level is high. This will replace the Standard Atmosphere profile, which has ~25 ppb ozone at ground level. We use measurements made during the NARSTO-NEOPS (North East Oxidant and Particle Study), which was an investigation of the coupling of the meteorological and chemical processes that control the evolution of air pollution events. The project included three major field programs carried out at a field site in northeast Philadelphia during the summers of 1998, 1999 and 2001.[27-29] An air pollution event on 21 August 1998 has been selected to evaluate the effective optical propagation conditions, vertically and horizontally, during these conditions. The case selected for the study is representative for the several air pollution events observed during the studies of the NARSTO NEOPS campaigns over five summers between 1998 and 2002 at a field site in Philadelphia PA. The largest ozone concentrations measured during the NARSTO NEOPS campaigns occurred on 3 July 1999 when the concentrations exceeded 130 ppb. The acquisition methods and analysis scheme are described in the references. Figure 7 shows a time sequence of water vapor, ozone, and extinction data from this day. A Raman lidar aimed vertically measures the Hartley-band absorption ratio between two Raman lines, N_2 (283.3 nm) and O_2 (277.6 nm), to determine the O_3 concentration. These daytime measurements are all made using the 4th harmonic of the Nd:YAG laser at 266 nm. The atmospheric reference enabled by the Raman lidar permits absolute measurements of extinction.

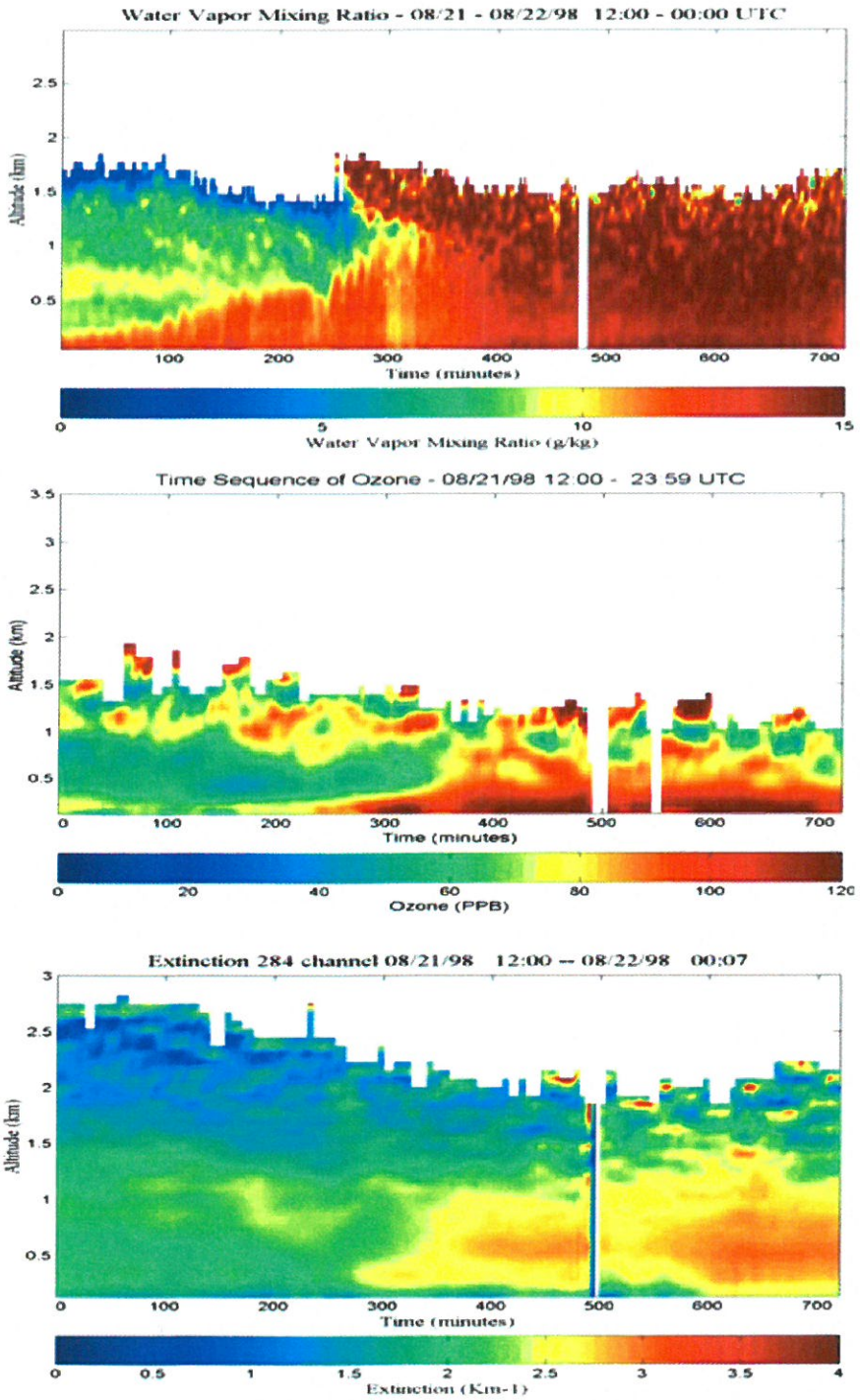

Figure 7. A 12 hour sequence (8 AM to 8 PM LT) of one-minute profiles smoothed with a 5-minute Hanning filter are shown for water vapor, ozone, and aerosol optical extinction during a major air pollution event that occurred on 21 August 1998. The vertical profiles are obtained by photon counting in 75 meter range bins and the profiles are terminated when the statistical error of photons counted within the 75-m X 5-min box exceeds 10%.

The particular time span of interest in this data set to extract the ozone profile used is indicated in Fig. 8. The ozone profile in Fig. 8(a) was averaged from a portion of the time-sequence of measurements shown in part (b). The time sequence covers from 5 AM until 3 PM local time. The profile was extracted as an average of the vertical profiles between the vertical blue lines in the plot, between 12:30 and 1:30 PM local time. Since the data from the lidar measurement is only available up to ~ 2 km, we use the USSA76 standard atmosphere profile for other altitudes. The highest measured point projects well onto the standard profile. In practice, our simulations are not calculated above 2 km, so the measured data is all that is used. We also note that the ground-level point of 96 ppb (mass) was taken from a point-measurement apparatus in simultaneous operation, and is slightly lower than the lowest lidar value due to ozone depletion processes active at ground level.

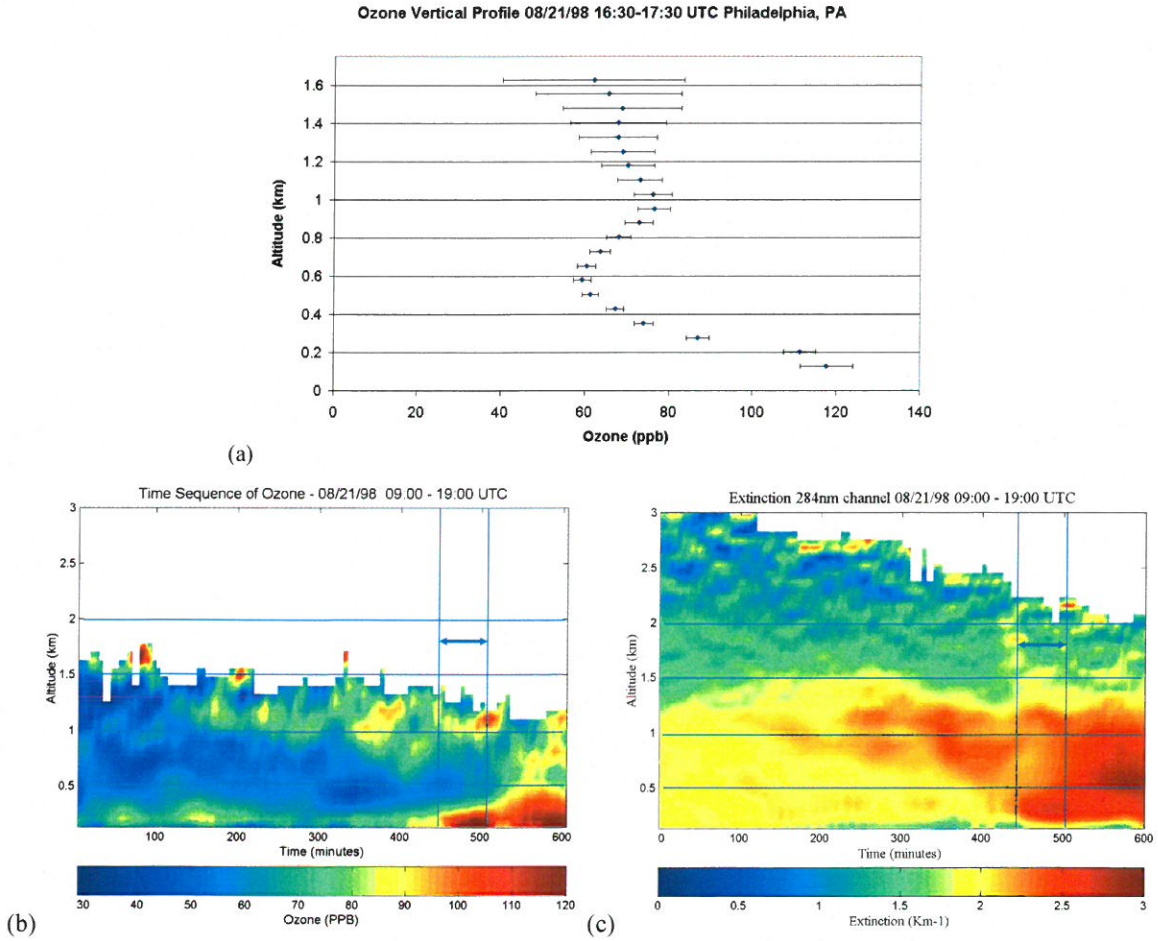

Figure 8. (a) The integrated profile of ozone shows the average concentration and 1-hour variability within each 75 meter range bin between 1630 and 1730 UTC (1230-0130 LT) on 21 August 1998. (b) The time sequence from which the ozone profile was extracted. The sequence of profiles was measured on 21 August 1998 0900-1900 UTC (0500-1500 LT) and shows the development of an air pollution event at the NARSTO-NEOPS site in Philadelphia. The data during the one hour time period between the two vertical blue lines was averaged to obtain the profile. (c) The simultaneously measured time dependent lidar profiles of the extinction at 284 nm are presented for comparison show the effects of small particle extinction associated with smog production from photochemical processes during that air pollution event. The lines show the smog extinction at time period of the ozone analysis above.

The result of replacing the standard atmosphere ozone profile with an extended version of the one in Fig. 8(a) in the MODTRAN calculation is shown in Fig. 9. The gain is reduced somewhat in the region of ozone absorption (Fig. 5), but not as dramatically as one might expect for such a significant pollution event. In fact, the elevated path calculation result is hardly changed from the standard atmosphere based calculation. This is because the ozone produced in the pollution

event stays relatively close to the ground as can be seen in the time sequences of profiles. The aerosols also created during the pollution event do not remain as close to the surface, but are mixed throughout the planetary boundary layer, for which water vapor acts as a tracer (Fig. 7).

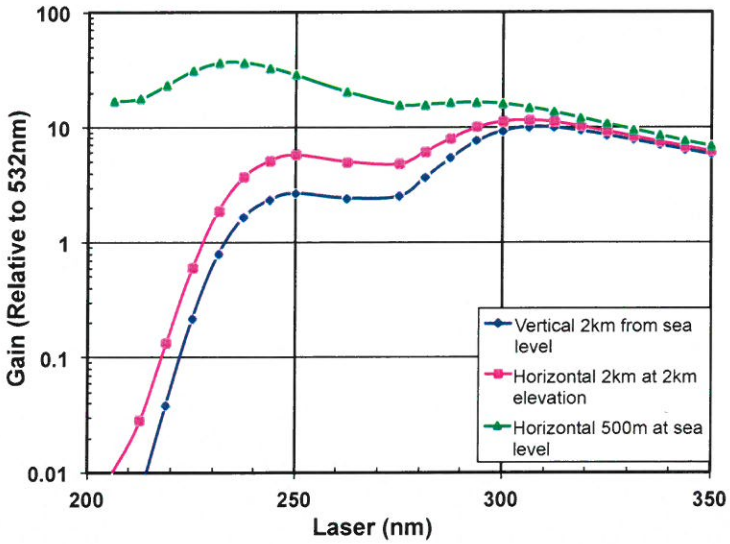

Figure 9. The effects of increased ozone concentration on the signal gain due to water pre-resonance in the presence of atmospheric absorption.

5. DISCUSSION

In all cases studied, the net gains for water vapor Raman actual signal levels are large for short path lengths, and reach a maximum of ~30 for a 500 meter long path at ~240 nm excitation wavelength. At shorter wavelengths, oxygen absorption strongly reduces the signal level. Longer path lengths (2 km here) are subject to more absorption losses, and the net gain peaks near the 310 nm excitation wavelength. A shoulder at ~250 nm excitation might be useful for a multi-purpose system, but the relative gain is comparable or less than that at 350 nm excitation source. If a shorter wavelength laser is used, measurements of ozone concentration would most likely be required to correct for wavelength-dependent absorption for species whose Raman lines fall within the ozone absorption spectral range (Fig. 5). Higher laser power with good beam quality availability at 355 nm, along with no need to do ozone correction, suggests that the 355 nm excitation may be a better choice; however, the solar-blind wavelengths below 300 nm provide a major advantage for daytime measurements. It is interesting to consider what would happen for a different species, other than water vapor, with absorption energies at longer wavelengths (~200 nm or longer) when resonance could be more closely approached. The gains would be much larger and hence able to offset more path absorption. The conclusion in that case might be quite different, although the results here show that a correction for absorption may be required, thus absorbing species, such as ozone, would need to be measured.

6. CONCLUSIONS

We have found a relatively simple form of the pre-resonance enhancement of water vapor in the deep UV spectral region, and used it to model the competition between resonance and dipole related increases in Raman signal levels to the extinction related decreases calculated with MODTRAN. We find that the net gains are substantial (>10X) for water vapor Raman actual signal levels for short path lengths, but absorption on longer path lengths reduces the net gains and shifts the optimal excitation wavelength to larger values, such as 355 nm. Measurements of ozone concentration would likely be required to correct for wavelength-dependent absorption due to ozone when shorter excitation wavelengths (250-270 nm) are used.

REFERENCES

[1] Sedlacek, A., Chen, C., "Exploitation of resonance Raman spectroscopy as a remote chemical sensor," *BNL-61359: Conf. 950787-35,* (1995).

[2] Sedlacek, A., Chen, C., "Remote detection of trace effluents using resonance Raman spectroscopy," *BNL-49542: Conf. 9311173-2,* (1995).

[3] Chen, C., Heglund, D., Ray, M., Harder. D., Dobert, R., Leung, K., Wu, M., Sedlacek, A., "Application of resonance Raman lidar for chemical species identification," *BNL-64388: Conf.-970465-19,* (1997).

[4] Sparks, R.G., Enloe, W.S., and Paesler, M.A., "Micro-Raman depth analysis of residual stress in machined germanium," Precision Engineering **13** (3), 189-195 (1991).

[5] Chadwick, C. T., Willitsford, A. H., Hallen, H. D., and Philbrick, C. R., "Deep ultraviolet Raman spectroscopy: a resonance-absorption trade-off illustrated by diluted liquid benzene," *J. Appl. Phys.*, **118**, 243101 (2015), http://dx.doi.org/10.1063/1.4938531.

[6] Hallen, H.D., "Nano-Raman Spectroscopy: Surface Plasmon Emission, Field Gradients, and Fundamentally Near Field Propagation Effects," NanoBiotechnology **3** (3), 197 (2009).

[7] Jahncke, C.L., Paesler, M. A., and Hallen, H.D., "Raman imaging with near-field scanning optical microscopy," Appl. Phys. Lett. **67** (17), 2483-2485 (1995).

[8] Willitsford, A., Chadwick, C. T., Hallen, H., and Philbrick, C. R., "Resonance Raman measurements utilizing a tunable deep UV source," *Proc. SPIE Laser Radar Technology and Applications XIII. 6950*-10, 8pp (2008).

[9] Willitsford, A., "Resonance Raman Spectroscopy in the Ultraviolet using a Tunable Laser," Penn State University Ph.D. Dissertation, (2008) https://etda.libraries.psu.edu/paper/8149/.

[10] Chadwick, C. T., "Resonance Raman Spectroscopy Utilizing Tunable Deep Ultraviolet Excitation for Materials Characterization," North Carolina State University Ph.D. Dissertation, (2009), http://repository.lib.ncsu.edu/ir/bitstream/1840.16/5473/1/etd.pdf .

[11] Adam Willitsford, C. Todd Chadwick, Hans Hallen, Stewart Kurtz, and C. Russell Philbrick, "Resonance Enhanced Raman Scatter in Liquid Benzene at Vapor-Phase absorption Peaks," Optics Express Vol. 21, No. 22, pp. 26150–26161 (2013).

[12] Ziegler, L. and Hudson, B., "Resonance Raman scattering of benzene and benzene-d_6 with 212.8 nm excitation," J. Chem. Phys. **74** (2), 982-992 (1981).

[13] Asher, S. and Johnson, C., "Resonance Raman excitation profile through the $^1B_{2u}$ state of benzene," J. Phys. Chem. **89**, 1375-1379 (1985).

[14] Gerrity, D., Ziegler, L., Kelly, P., Desiderio, R., and Hudson, B., "Ultraviolet resonance Raman spectroscopy of benzene vapor with 220-184 nm excitation," J. Chem. Phys. **83** (7), 3209-3213 (1985).

[15] Sension, R., Brudzynski, R., Li, S., and Hudson, B., "Resonance Raman spectroscopy of the B_{1u} region of benzene: analysis in terms of pseudo-Jahn-Teller Distortion," J. Chem. Phys. **96** (4), 2617-2628 (1991).

[16] Sension, R., Brudzynski, R., and Hudson, B., "Vacuum ultraviolet resonance Raman studies of the valence electronic states of benzene and benzene-d_6: The E_{1u} state and a putative A_{2u} state," J. Chem. Phys. **94** (2), 873-882 (1990).

[17] Ziegler, L. and Albrecht, A., "Raman scattering of benzene in the ultraviolet," J. Chem. Phys. **67** (6), 2753-2757 (1977).

[18] Li, Ling, Lim, Shuang Fang, Puretzky, Alexander, Riehn, Robert, and Hallen, Hans, "Near-field enhanced ultraviolet resonance Raman spectroscopy using aluminum bow-tie nano-antenna," *Appl. Phys. Lett.* **101** (11), (2012) DOI: 10.1063/1.4746747.

[19] Hallen, Hans D., Niu, Shupeng and Li, Ling, "Time and neighbor interaction in resonance Raman spectroscopy," Proc. SPIE Ultrafast Imaging and Spectroscopy II, 9198, (2014).

[20] Hallen, Hans D., Neely III, Ryan R., Willitsford, Adam H., Chadwick, C. Todd, Philbrick, C. Russell, "Coherence in UV resonance Raman spectroscopy of liquid benzene and toluene, but not ice," Proceedings SPIE Ultrafast Imaging and Spectroscopy, 8845, (2013) doi: 10.1117/12.2024313.

[21] Willitsford, Adam, Chadwick, C. Todd, Hallen, Hans, Kurtz, Stewart, Philbrick, C. Russell, "Resonance-Enhanced Raman Scattering of Ring-Involved Vibrational Modes in the 1B2u Absorption Band of Benzene, Including the Kekule Vibrational Modes v9 and v10," *J. Phys. Chem. A* **120**, 503–506 (2016) DOI: 10.1021/acs.jpca.5b08159.

[22] Philbrick, C. Russell; Hallen, Hans D.; "Laser remote sensing of species concentrations and dynamical processes," Proceedings SPIE Laser Radar Technology and Applications XIX **9080**, 9080OZ (2014) doi: 10.1117/12.2050696.
[23] Hallen, Hans D.; Willitsford, Adam; Weeks, Reagan; Philbrick, C. Russell; "UV resonance Raman signatures of phonon-allowed absorptions and phonon-driven bubble formation," Ultrafast Nonlinear Imaging and Spectroscopy III, **9584**, 95840P (2015) doi 10.1117/12.2188528.
[24] Sivakumar, T., Chew, H., and Johari, G., "Effect of pressure on the Raman Spectrum of ice," Nature **275**, (1978).
[25] Mishima, O. and Suzuki, Y., "Propagation of the polyamorphic transition of ice and the liquid-liquid critical point," Nature 419, (2002).
[26] Kapitan, J., Hecht, L., and Bour. P., "Raman Spectral evidence of methyl rotation in liquid toluene," Phys. Chem. Chem. Phys. **10**, 1003-1008 (2008).
[27] Philbrick CR, Ryan WF, Clark RD, Doddridge BG, Dickerson RR, Koutrakis P, Munger JW, McDow SR, Rao ST, Eatough DJ, Hopke PK, Dasgupta PK. "Overview of the NARSTO-NE-OPS Program," Proceedings of the American Meteorological Society 4th Conference on Atmospheric Chemistry, , 107-114 (2002) Illinois. UNT Digital Library. http://digital.library.unt.edu/ark:/67531/metadc738172/.
[28] Collier PJ, Unni S, Verghese SJ, Willitsford A, Philbrick CR, Clark RD, Doddridge BG. "Raman lidar measurements of tropospheric ozone," Proceedings of the American Meteorological Society 5th Conference on Atmospheric Chemistry, , 6.3 (2003).
[29] Esposito ST, Philbrick CR. "Raman/DIAL technique for ozone measurements," Proceedings of the Nineteenth International Laser Radar Conference, NASA/CP-1998-207671/PT1, 407-410 (1998).